PHYSICAL REVIEW E **90**, 031302(R) (2014)

Gibbs' principle for the lattice-kinetic theory of fluid dynamics

I. V. Karlin, F. Bösch, and S. S. Chikatamarla
Department of Mechanical and Process Engineering, ETH Zurich, 8092 Zurich, Switzerland
(Received 11 July 2014; published 30 September 2014)

Gibbs' seminal prescription for constructing optimal states by maximizing the entropy under pertinent constraints is used to derive a lattice kinetic theory for the computation of high Reynolds number flows. The notion of modifying the viscosity to stabilize subgrid simulations is challenged in this kinetic framework. A lattice Boltzmann model for direct simulation of turbulent flows is presented without any need for tunable parameters and turbulent viscosity. Simulations at very high Reynolds numbers demonstrate a major extension of the operation range for fluid dynamics.

DOI: 10.1103/PhysRevE.90.031302 PACS number(s): 47.11.−j, 05.20.Dd, 51.10.+y

The lattice Boltzmann (LB) method [1] is a modern and highly successful kinetic-theory approach to computational fluid dynamics and computational physics of complex flows and fluids, with applications ranging from turbulence [2] to flows at a micron scale [3] and multiphase flows [4], to relativistic hydrodynamics [5], soft-glassy systems [6], and beyond. The LB method numerically solves a fully discrete kinetic equation for populations $f_i(\boldsymbol{x},t)$, designed to reproduce the Navier-Stokes equations in the hydrodynamic limit. Populations correspond to discrete velocities $\boldsymbol{v}_i$, $i = 1,\ldots,b$, which fit into a regular spatial lattice with the nodes $\boldsymbol{x}$. This enables a simple and highly efficient "stream-along-links-and-equilibrate-at-nodes" realization of the LB algorithm. Focusing on the classical case of the incompressible fluid dynamics, a general form of the LB equation may be written,

$$f_i(\boldsymbol{x}+\boldsymbol{v}_i,t+1) = f_i' \equiv (1-\beta) f_i(\boldsymbol{x},t) + \beta f_i^{\mathrm{mirr}}(\boldsymbol{x},t). \quad (1)$$

Here the left-hand side is the propagation of the populations along the lattice links, while the right-hand side is the so-called postcollision state f'.

The key is the mirror state, f^{mirr}. Realization of hydrodynamics was made possible, in the first place with the lattice Bhatnagar-Gross-Krook (LBGK) model [7,8], in which one takes

$$f_i^{\mathrm{mirr}} = 2 f_i^{\mathrm{eq}} - f_i. \quad (2)$$

Here f_i^{eq} is the equilibrium which is found as a maximizer of the entropy,

$$S[f] = -\sum_{i=1}^{b} f_i \ln\left(\frac{f_i}{W_i}\right), \quad (3)$$

subject to fixed locally conserved fields, $\rho = \sum_{i=1}^{b} f_i$ (density) and $\rho\boldsymbol{u} = \sum_{i=1}^{b} \boldsymbol{v}_i f_i$ (momentum density), and where the weights W_i are lattice-specific constants. With the proper symmetry of the lattice, the LBGK equation, (1) and (2), recovers the Navier-Stokes equation for the fluid velocity $\boldsymbol{u}$, with the kinematic viscosity ν,

$$\nu = c_s^2\left(\frac{1}{2\beta} - \frac{1}{2}\right), \quad (4)$$

where c_s is the speed of sound [a lattice dependent $O(1)$ constant]. The form of the mirror state (2) is known as the over-relaxation. Note that the LBGK model is unambiguous since $\beta \in [0,1]$ is fixed by the kinematic viscosity (4). The most important limit is $\beta \to 1$ (small kinematic viscosity) as it is pertinent to achieving, if only in principle, high Reynolds number regimes.

Almost immediately after its inception, the LBGK model has taken lead in the lattice Boltzmann approach to the simulation of complex hydrodynamic phenomena [1,9], and remains the "working horse" of the LB methods to date. The popularity of LBGK is primarily based on its simplicity and exceptional computational efficiency. It is unfortunate, and was soon realized, that LBGK shows severe deficiencies (disruptive numerical instability) already at relatively low Reynolds numbers. This precluded the LB method to make a sustainable impact in the field of computational fluid dynamics. A new, physically transparent LB model is critically needed to replace the LBGK [1].

This long-due lattice kinetic model for high Reynolds numbers is reported in this Rapid Communication. The key physical principle in its construction dates back to Gibbs [10] who described optimal (equilibrium) states as points of entropy maximum under relevant constraints. In our case, the optimal mirror states of LB are constructed by maximizing the discrete entropy function (3) under the constraints of over-relaxation of the hydrodynamic stresses. The resulting LB model outperforms LBGK by orders of magnitude in terms of attainable Reynolds numbers. On the practical side, the analytical formula for the optimal mirror state derived herein adds only a small computational overhead, thus retaining the simplicity and efficiency of LB models. This model was vigorously tested in a number of two- and three-dimensional benchmark flow situations, including simulation of flow past bluff bodies at very high Reynolds numbers. The main steps of the derivation are given below for any admissible lattice [11], whereas all practical formulas for the two-dimensional realization are presented in the Supplemental Material [12].

We begin with a remark that populations can be equivalently represented in terms of moments (a set of b linearly independent combinations of f_i's). Then we can write

$$f_i = k_i + s_i + h_i, \quad (5)$$

where k_i (=kinematic part) depends only on the locally conserved fields, s_i (=shear part) depends on the stress tensor $\boldsymbol{\Pi} = \sum_{i=1}^{b} \boldsymbol{v}_i \otimes \boldsymbol{v}_i f_i$, and h_i (=higher-order moments) is a linear combination of the remaining higher-order moments.

Representation (5) is easily obtained for any lattice and any moment basis (see Supplemental Material [12]). For now, it suffices to mention that s_i is a linear combination of $D(D+1)/2$ functions $\Pi_{\alpha\beta}$ (D is space dimension), and h_i is a linear combination of the remaining $b-(D+1)(D+2)/2$ higher-order moments.

With the representation (5), a different mirror state can be sought in a one-parameter form,

$$f_i^{\rm mirr} = k_i + \left[2s_i^{\rm eq} - s_i\right] + \left[(1-\gamma)h_i + \gamma h_i^{\rm eq}\right], \qquad (6)$$

where γ is a parameter which is not yet specified. We note that, when (6) is used in (1), one arrives at nothing but a special (not the most general) LB model of the type considered earlier by many authors for various choices of the moment basis [13–15]. For any γ, the resulting LB model still recovers hydrodynamics with the same kinematic viscosity ν (4). A similar idea was widely used in the LB literature to extend the stability range of LBGK ($\gamma = 2$), by using multiple relaxation times (MRT) that do not affect the over-relaxation of stresses s_i. The MRT models were successful in moderately stabilizing the LB method but still remain challenged by high Reynolds numbers [16]. Note that Eqs. (1) and (6) can also be rewritten as $f_i' = f_i + 2\beta(f_i^{\rm GE} - f_i)$, with the generalized equilibrium [17–19] of the form $f_i^{\rm GE} = f_i^{\rm eq} + (1/2)(\gamma-2)(h_i^{\rm eq} - h_i)$.

The proposal (6) is a family of possible mirror states, and the most crucial question is how to choose the *stabilizer* γ in order to achieve better performance at small kinematic viscosity ($\beta \to 1$). At first glance, it seems plausible to set $\gamma = 1$ ("relax" the higher-order degrees of freedom h to their equilibrium $h^{\rm eq}$; see, e.g., [20]). However, in many benchmark flow situations no improvement is achieved. Hence, just the proposal (6) is incomplete because it does not readily answer the above question of how to find an optimal mirror state (6).

The major change of perspective here is that the stabilizer γ should *not* be considered as a "tunable" parameter. Rather, it has to be put under entropy control and *computed by maximizing the entropy* in the postcollision state f'. This matches the physics of the problem at hand, since constrained equilibria correspond to the maximum of the entropy (here the constraint is that the stress part remains fixed by the over-relaxation, $s_i^{\rm mirr} = 2s_i^{\rm eq} - s_i$).

Specifically, let $S(\gamma)$ be the entropy of the postcollision states appearing in the right-hand side of (1), with the mirror state (6). Then we require that the stabilizer γ corresponds to the maximum of this function. Introducing deviations $\Delta s_i = s_i - s_i^{\rm eq}$ and $\Delta h_i = h_i - h_i^{\rm eq}$, the condition for the critical point reads

$$\sum_{i=1}^{b} \Delta h_i \ln\left(1 + \frac{(1-\beta\gamma)\Delta h_i - (2\beta-1)\Delta s_i}{f_i^{\rm eq}}\right) = 0. \qquad (7)$$

Equation (7) suggests that among all nonequilibrium states with the fixed mirror values of the stress, $s_i^{\rm mirr} = 2s_i^{\rm eq} - s_i$, we pick the one which maximizes the entropy. Note that, in this way defined *entropic stabilizer* γ appears not as a tunable parameter but rather it is computed on each lattice site at every time step from Eq. (7). Thus, the entropic stabilizer self-adapts to a value given by the maximum entropy condition (7).

In order to clarify the properties of the solution to Eq. (7), let us introduce the entropic scalar product $\langle X|Y\rangle$ in the b-dimensional vector space,

$$\langle X|Y\rangle = \sum_{i=1}^{b} \frac{X_i Y_i}{f_i^{\rm eq}}, \qquad (8)$$

and expand in (7) to the first nonvanishing order in $\Delta s_i/f_i^{\rm eq}$ and $\Delta h_i/f_i^{\rm eq}$ to obtain

$$\gamma^* = \frac{1}{\beta} - \left(2 - \frac{1}{\beta}\right)\frac{\langle \Delta s|\Delta h\rangle}{\langle \Delta h|\Delta h\rangle}. \qquad (9)$$

The result (9) explains the mechanism of failure of the proposal $\gamma \approx 1$ at $\beta \approx 1$: Whenever vectors Δs and Δh are nonorthogonal (in the sense of the entropic scalar product), the deviation of γ^* from $\gamma = 1$ may become very significant. Indeed, in (9), the *correlation* between the shear and the higher-order parts $\sim\langle \Delta s|\Delta h\rangle$ is not a correction to $\gamma = 1$ but rather a contribution of the same order $O(1)$. Below, we shall discuss why the estimate (9) is valid for high Reynolds numbers.

The present LB scheme with the entropic stabilizer was realized in two and three dimensions (see Supplemental Material [12] for the $D = 2$ lattice with $b = 9$ discrete velocities). For a benchmark, a perturbed double periodic shear layer flow was used, with initial conditions [21]

$$u_x = \begin{cases} U\tanh\left[\lambda\left(y/L - 0.25\right)\right], & y \leqslant L/2, \\ U\tanh\left[\lambda\left(0.75 - y/L\right)\right], & y > L/2, \end{cases}$$

$$u_y = \delta U \sin\left[2\pi\left(x + 0.25\right)\right].$$

Here L is the number of grid points in both x and y directions, and periodic boundary conditions are applied in both directions. Varying the parameter λ alters the width of the shear layers, and this is fixed at $\lambda = 80$ (thin layer case). The velocity perturbation in the y direction initiates a Kelvin-Helmholtz instability causing the roll up of the antiparallel shear layers. The parameter δ controls the size of the initial perturbation and is fixed here at $\delta = 0.05$. U determines the magnitude of the initial x velocity. The Reynolds number is defined as $\mathrm{Re} = UL/\nu$; the velocity amplitude $U = 0.04$ was used.

Figure 1 demonstrates a snapshot of the roll up on a fine grid $L = 512$ at time $t = 1$ ($t = TU/L$, where T is the number of lattice time steps). The solution to (7) was found by Newton-Raphson iteration at each lattice node at every time step. While the simulation excellently reproduces the expected shape of the vortex [21], the corresponding snapshot of the spatial distribution of the entropic stabilizer γ is also shown in Fig. 1. It is clear that the entropic stabilizer is far from any fixed value, moreover both positive and negative values of γ are present. Note that, the computed values of the entropic stabilizer γ are not necessarily confined to the so-called linear stability interval [0,2]. This clearly shows that the present new model is far from any LB model with a fixed γ, even in a well resolved simulation. Amazingly, as the result of the self-adaptation, the spatial distribution of γ follows the pattern of the developing vortex.

For the stability analysis, a coarse grid was used, $L = 128$. At this grid size, the standard LBGK scheme becomes numerically unstable at $\mathrm{Re} \approx 20 \times 10^3$. Moreover, the choice $\gamma = 1$ in (6) does not bring any improvement on the stability. In

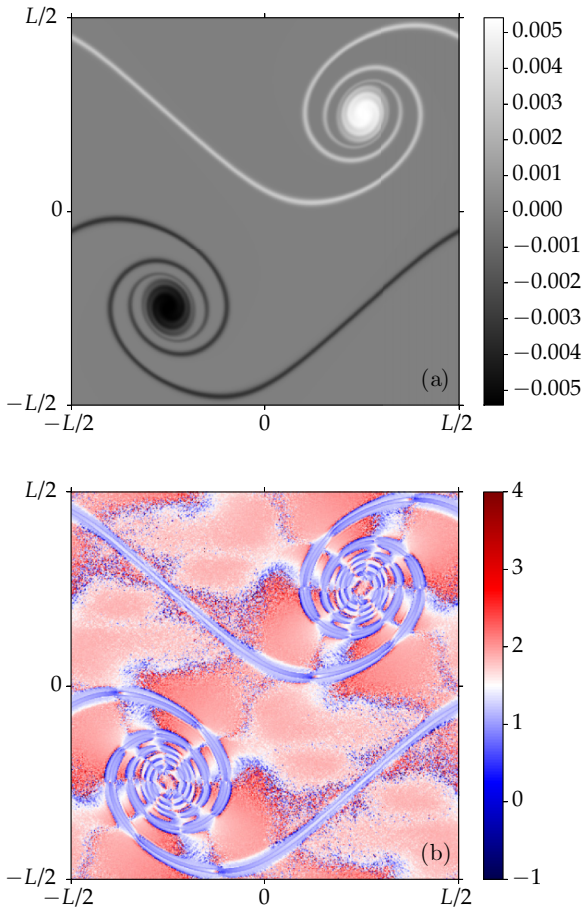

FIG. 1. (Color online) Roll up of the double shear layer. Grid $L = 512$, $\mathrm{Re} = 30\,000$. (a) Snapshot of the vorticity at $t = 1$. (b) Distribution of the entropic stabilizer γ.

contrast to this, the present scheme delivers stable simulation all the way up to high Reynold numbers, till at least $\mathrm{Re} \sim 10^7$. In Fig. 2, the history of the total entropy $S_{\mathrm{tot}}(t) = \sum_{\boldsymbol{x}} S[f(\boldsymbol{x},t)]$ is shown for the four LB models: the LBGK, the LB model with $\gamma = 1$, the entropic LBGK (ELBGK) model

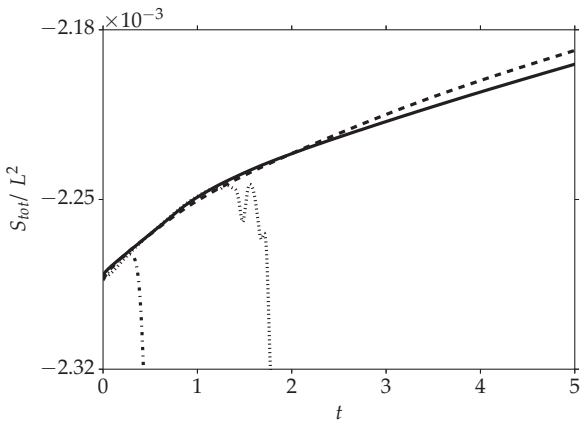

FIG. 2. History of the total entropy in the simulation of the double shear layer. Solid: present LB; dashed: ELBGK; dotted: LB with $\gamma = 1$; dash-dotted: LBGK. Grid size: $L = 128$; Reynolds number $\mathrm{Re} = 30\,000$.

[22], and the present LB with the entropic stabilizer. Collapsing of the former two models is accompanied by the unbounded decay of S_{tot}, whereas the latter two LB schemes (the present and the ELBGK) demonstrate monotonic and very similar growth of the total entropy.

Moreover, evaluations of the entropic stabilizer via numerically solving Eq. (7) were found in excellent agreement with the analytical formula (9). This is not surprising. Indeed, the LB models are valid for high Reynolds numbers rather than for the low ones [1]. This is obvious from the von Kármán relation, $\mathrm{Re} = \mathrm{Ma}/\mathrm{Kn}$, where $\mathrm{Ma} = U/c_{\mathrm{s}}$ is the Mach number and $\mathrm{Kn} = \nu/c_{\mathrm{s}}L$ is the Knudsen number. The hydrodynamic limit is valid at $\mathrm{Kn} \to 0$. Thus, large Re implies small deviations from the local equilibrium. Close to the local equilibrium, the entropy in the postcollision state $\Delta S = S[f'] - S[f^{\mathrm{eq}}]$ is a quadratic function ($\beta = 1$ for simplicity),

$$\Delta S(\gamma) = -\frac{(1-\gamma)^2}{2}\langle \Delta h|\Delta h\rangle + (1-\gamma)\langle \Delta s|\Delta h\rangle - \frac{1}{2}\langle \Delta s|\Delta s\rangle. \tag{10}$$

The maximum of this parabola returns γ^* (9). If the Δs and Δh parts happen to be uncorrelated, $\langle \Delta s|\Delta h\rangle = 0$, the entropic stabilizer returns $\gamma = 1$. It is only in this case that the maximum of the entropy in the postcollision state is achieved by the "relaxation," $h' = h^{\mathrm{eq}}$. However, any correlation between the s and h parts shifts the maximum entropy postcollision state h' away from h^{eq}. Close to the local equilibrium, this shift is simply proportional to the relative strength of the correlation, $\langle \Delta s|\Delta h\rangle/\langle \Delta h|\Delta h\rangle$. The entropy in the maximum entropy state is always higher than in the "relaxed" state:

$$\Delta S(\gamma^*) - \Delta S(1) = \frac{\langle \Delta s|\Delta h\rangle^2}{2\langle \Delta h|\Delta h\rangle} \geqslant 0. \tag{11}$$

These arguments explain why γ^* (9) is a physically relevant entropy control rather than a mere approximation to (7). *Hence, in all the subsequent simulations, only the analytical formula (9) was used.* The computational overhead of the present model

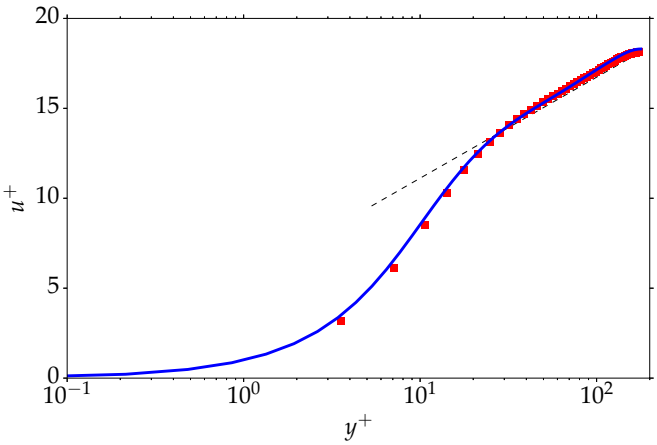

FIG. 3. (Color online) Average streamwise velocity in wall units in the simulation of the turbulent channel flow at $\mathrm{Re}_\tau = 180$. Symbol: present LB model; solid line: DNS data [25]. The log-law of wall (dashed) is shown as a guide to the eye.

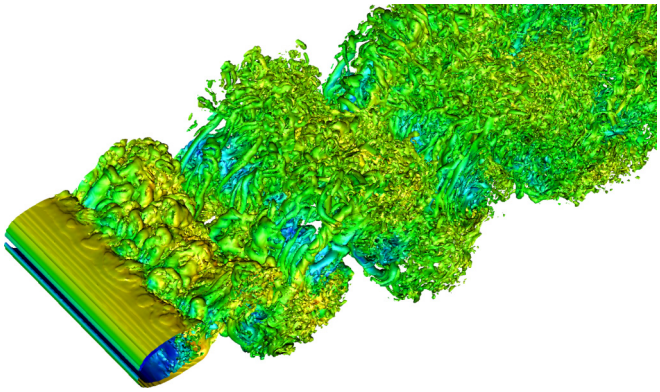

FIG. 4. (Color online) Snapshot of a fully developed turbulent flow past a round cylinder at Re = 140 000. Vorticity isosurface is shown colored with the velocity magnitude.

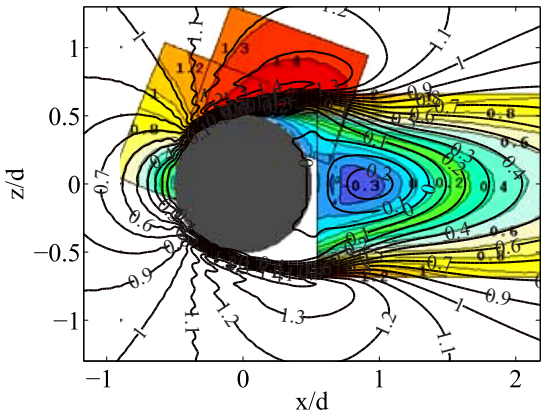

FIG. 5. (Color online) Averaged streamwise reduced velocity u_x/U. Lines: simulation; shaded: experiment [27].

compared to an implementation with a fixed γ is only about 10%. If compared to standard LBGK the amount of work is larger as $D(D+1)/2$ moments $\mathbf{\Pi}$ have to be computed additionally which results in an overhead of about two times.

The present method is extended to three dimensions in a straightforward way, and was realized on the standard lattice with $b = 27$ discrete velocities. First, we considered the Kida vortex flow which was extensively studied previously using LB methods [23,24]. Simulation on the coarse grid (periodic box with the side $L = 100$) confirmed stability observed in two dimensions (simulations were stable till at least Re $\sim 10^9$).

In order to confirm the accuracy of the present LB model in coarse-grid simulations, we present the result for the standard benchmark of the turbulent channel flow. In Fig. 3, the average streamwise velocity profile for the uniform grid resolution $\Delta^+ \approx 3.5$ at $\mathrm{Re}_\tau \approx 180$ is compared with the direct numerical simulation (DNS) data [25]. Agreement is excellent, especially in the log-law regime (cf., e.g., [26]).

Finally, in order to validate that the present LB model is compatible with the existing boundary conditions, we run the simulation of the flow past a round cylinder. The Reynolds number is $\mathrm{Re} = Ud/\nu$, where d is the diameter of the cylinder, and U is the uniform inlet velocity. The grid of the size $X = 45d$ (streamwise), $Y = 5d$ (spanwise) and $Z = 20d$ (vertical) was used in the simulation, with $d = 30$ lattice spacings. Boundary conditions described in [26] were used on the cylinder surface. No-boundary condition was applied at the outlet, free slip at the top and the bottom sides, and periodic boundary condition in the span direction. A snapshot of the vorticity field of the fully developed three-dimensional turbulent flow at $\mathrm{Re} = 1.4 \times 10^5$ is shown in Fig. 4. Results were compared with particle image velocimetry measurements of the near-wake velocity field at the same Reynolds number reported in [27]. In Fig. 5, the averaged streamwise velocity contours are overlapped with the experimental data of Ref. [27].

A comparison between the present simulation and experimental data provides compelling evidence of increased stability and good accuracy of our model. Such simulations were hitherto not possible without the use of subgrid turbulence models. These results will be expanded in our subsequent publications.

In summary, we proposed a different perspective on the direct simulation of low-dissipative hydrodynamic flows using advanced fluid-kinetic theory. Entropy control, with its solid physical background, significantly extends the operation range of the lattice Boltzmann method, with only a minute computational overhead for the evaluation of formula (9). No tunable parameters, considerably higher stability, and ease in the implementation are the salient features of this LB model. Based on these observations, we believe that this approach will find attractive applications in the emergent fluid-kinetic approaches to complex flows and fluids, ranging from turbulence to multiphase flows [4], to relativistic hydrodynamics [5], soft-glassy systems [6], and beyond.

This work was supported by the European Research Council (ERC) Advanced Grant No. 291094-ELBM. Computational resources at the Swiss National Super Computing Center CSCS were provided under Grants No. S492 and No. S468.

[1] S. Succi, *The Lattice Boltzmann Equation for Fluid Dynamics and Beyond* (Oxford University Press, Oxford, 2001).

[2] H. Chen, S. Kandasamy, S. Orszag, R. Shock, S. Succi, and V. Yakhot, Science **301**, 633 (2003).

[3] S. Ansumali, I. V. Karlin, S. Arcidiacono, A. Abbas, and N. I. Prasianakis, Phys. Rev. Lett. **98**, 124502 (2007).

[4] M. R. Swift, W. R. Osborn, and J. M. Yeomans, Phys. Rev. Lett. **75**, 830 (1995).

[5] M. Mendoza, B. M. Boghosian, H. J. Herrmann, and S. Succi, Phys. Rev. Lett. **105**, 014502 (2010).

[6] R. Benzi, S. Chibbaro, and S. Succi, Phys. Rev. Lett. **102**, 026002 (2009).

[7] H. Chen, S. Chen, and W. H. Matthaeus, Phys. Rev. A **45**, R5339 (1992).
[8] Y.-H. Qian, D. d'Humieres, and P. Lallemand, Europhys. Lett. **17**, 479 (1992).
[9] C. K. Aidun and J. R. Clausen, Annu. Rev. Fluid. Mech. **42**, 439 (2010).
[10] J. W. Gibbs, *Elementary Principles in Statistical Mechanics* (Charles Scribner's Sons, New York, 1902).
[11] S. S. Chikatamarla and I. V. Karlin, Phys. Rev. Lett. **97**, 190601 (2006).
[12] See Supplemental Material at http://link.aps.org/supplemental/10.1103/PhysRevE.90.031302 for details of the derivation of the model in two dimensions.
[13] F. Higuera, S. Succi, and R. Benzi, Europhys. Lett. **9**, 345 (1989).
[14] D. d'Humières, in *Rarefied Gas Dynamics: Theory and Simulations*, edited by B. D. Shizgal and D. P. Weaver, AIAA Prog. Aeronaut. Astronaut Vol. 159 (AIAA, Washington, DC, 1992), pp. 450–458.
[15] M. Geier, A. Greiner, and J. G. Korvink, Phys. Rev. E **73**, 066705 (2006).
[16] R. K. Freitas, A. Henze, M. Meinke, and W. Schroeder, Comput. Fluids **47**, 115 (2011).
[17] P. Asinari and I. V. Karlin, Phys. Rev. E **79**, 036703 (2009).
[18] P. Asinari and I. V. Karlin, Phys. Rev. E **81**, 016702 (2010).
[19] I. Karlin, P. Asinari, and S. Succi, Philos. Trans. R. Soc., A **369**, 2202 (2011).
[20] J. Latt, Ph.D. thesis, University of Geneva, 2007.
[21] M. L. Minion and D. L. Brown, J. Comput. Phys. **138**, 734 (1997).
[22] I. V. Karlin, A. Ferrante, and H. C. Öttinger, Europhys. Lett. **47**, 182 (1999).
[23] B. Keating, G. Vahala, J. Yepez, M. Soe, and L. Vahala, Phys. Rev. E **75**, 036712 (2007).
[24] S. S. Chikatamarla, C. E. Frouzakis, I. V. Karlin, A. G. Tomboulides, and K. B. Boulouchos, J. Fluid Mech. **656**, 298 (2010).
[25] R. D. Moser, J. Kim, and N. N. Mansour, Phys. Fluids **11**, 943 (1999).
[26] S. S. Chikatamarla and I. V. Karlin, Physica A **392**, 1925 (2013).
[27] R. Perrin, M. Braza, E. Cid, S. Cazin, F. Moradei, A. Barthet, A. Sevrain, and Y. Hoarau, Flow, Turbul. Combust. **77**, 185 (2006).